"Invisible" ligands stabilize colloidal melanin particles – the case of L-DOPA

Koen P. Vercruysse, Venise Govan and Jaila Winford
Chemistry department, Tennessee State University, Nashville, TN USA
kvercruysse@tnstate,edu

Abstract

This report details observations that the *in vitro* synthesis of L-DOPA-based melanin leads to a two-component material: dark-colored aggregates stabilized by colorless ligands. Despite the appearance of dissolution, the melanin materials generated behave as dispersed, colloidal particles. All dispersible materials can, in part, be aggregated and precipitated through the addition of mono- or multivalent cations but in a non-linear, concentration-dependent fashion. The addition of cationic species, at sufficiently high concentrations, fractionates the colloids into a dark precipitate and a dispersible, colorless fraction. Precipitated aggregates could be redispersed in water through the addition of sufficiently high concentrations of KCl; an additional indicator of their colloidal nature. The dispersible fraction exhibits absorbance in the UVA and UVB range of the electromagnetic spectrum, but little to no absorbance in the visible range. The fractionated melanins were characterized using liquid chromatography, UV-Vis and FT-IR spectroscopy. Based upon the results presented we suggest a model for synthetic melanins as colloidal particles built from a dark-colored core aggregate stabilized by a set of colorless ligands.

1. Introduction

Despite decades of research the class of pigments known as melanins (MN) remains an enigmatic group of biomolecules. Their molecular structure and physic-chemical properties are currently not completely established. As functionality is related to structure it is difficult to systematically explore the properties and potential applications of these biomolecules. Extensive reviews on the structure, properties and potential applications have been written by several authors in recent years.[1-6] In human (and other animal) physiology two distinct classes of MNs are responsible for the coloration of the skin and hair: eumelanin (EuMN) and pheomelanin (PhMN).[7-8] EuMN is typically described as a brown to black colored material built from L-DOPA as the precursor. PhMN is typically described as a yellow to red pigment built through a

combination of L-DOPA and the amino acid cysteine (C). The biochemical pathways that lead to these two different classes of MN are described by the classic Raper-Mason scheme.[9-10] In this scheme, L-DOPA undergoes oxidation and cyclization to intermediates like 5,6-dihydroxyindole (DHI) and 5,6-dihydroxyindole-2-carboxylic acid (DHICA) which then yield the final EuMN material. In the presence of C, the pathway is diverted to a different set of intermediates, e.g., 5-S-cysteinyl-DOPA, 1,4-benzothiazine (BTZ) or 1,4-benzothiazine-3-carboxylic acid (BTZCA), which then lead to the final PhMN material.[11] Another type of MN, termed neuromelanin, built from dopamine with or without C, is found in select areas of the brain.[12-14] In addition to L-DOPA and dopamine, various other precursors can be and are used as precursors for MN-like materials as reviewed elsewhere.[6]

This report details ongoing explorations on the physic-chemical properties of MNs by evaluating the interaction between synthetic MNs and a multitude of cationic species. The studies described herein suggest that MN-like materials, despite sometimes appearing as dissolved, are dispersed, colloidal entities. “Insoluble” MN materials can be “dissolved” through the addition of KCl or other salts, while “soluble” MN materials can be aggregated or precipitated by the addition of various salts. In addition, the results from these studies provide additional evidence that the *in vitro* synthesis of MNs leads to a hybrid material composed of at least two sets of components.[15-16]

2. Experimental

2.1. Materials

L-Dihydroxyphenylalanine (L-DOPA), NaCl, KCl, $CaCl_2.2H_2O$, $MgCl_2$, $MnCl_2.4H_2O$, $CoCl_2.6H_2O$, $CuCl_2.2H_2O$, $EuCl_3.6H_2O$ and $LaCl_3.7H_2O$ were obtained through Fisher Scientific (Waltham, MA). All other reagents were of analytical grade.

2.2 Synthesis of MN materials

MN materials were synthesized by dissolving L-DOPA in 50mM Na-acetate buffer (pH=6.4) followed by the addition of 50mM Na_2CO_3 to a ratio of 50:50 (v/v) buffer/Na_2CO_3. Two reactions were set up: one containing about 700mg L-DOPA in 100mL (35mM) termed HiC reaction and one containing about 200mg L-DOPA in 100mL (10mM) termed LoC reaction. After three to four days of reaction at room temperature the crude reaction mixtures were

dialyzed and lyophilized. During the reaction and subsequent dialysis process the HiC reaction exhibited aggregations, while this was not visible for the LoC reaction. The dried materials from both reactions could not entirely be redispersed in water. The materials were redispersed in water to a concentration of 10 mg/mL (w/v) and centrifuged. The supernatants were collected and lyophilized and termed the dispersible fraction (F_{disp}). The precipitates were repeatedly washed with water and lyophilized and termed the precipitated fraction (F_{prec}).

2.3 Cation precipitation and dispersion experiments

F_{disp} materials were dispersed in water at a concentration of 1 mg/mL. To 500µL of this mixture, 50µL cation solution was added, and the combination was kept at room temperature for 24 hours. Following centrifugation, the absorbance of the supernatant between 350 and 900nm was measured and select aliquots were diluted fourfold for HPLC analysis.

F_{prec} materials were dispersed at a level of 1 mg/mL with a) water, b) 50mM KCl, c) 250mM KCl and d) 500mM KCl. After standing overnight at room temperature, photographs of the mixtures were taken. Following centrifugation, absorbance spectra of the supernatants were recorded, and aliquots were diluted fourfold for HPLC analysis.

2.4 Other analyses and techniques

UV-Vis spectroscopy, FTIR spectroscopy, RP-HPLC analyses, dialysis and freeze drying were performed as outlined elsewhere.[15-18] An exception is the RP-HPLC analyses which were performed at a flow rate of 0.5 mL/min instead of 1 mL/min to improve resolution.

3. Results

3.1 Characterization of materials

3.1.1 UV-Vis absorbance spectra

Quantitative estimates of the "darkness" of any sample were calculated by integrating, between 400 and 900nm, the absorbance spectrum of the sample fitted with an exponential function and calculating the area-under-the-curve (AUC) as outlined elsewhere and shown in **eq.1**.[17]

$$AUC = \int_{400}^{900} A_0 * \ e^{-k\lambda} d\lambda = \frac{A_0}{-k} * (e^{-k*900} - e^{-k*400}) \qquad \textbf{eq.1}$$

In this equation, k is the decay constant of the exponential profile of the absorbance (A) as a function of the wavelength (λ). In addition, to distinguish EuMN-like materials from PhMN-like materials, the ratio of the absorbance at 650nm over the absorbance at 500nm (A_{650}/A_{500}) was evaluated. Although these two wavelengths are arbitrarily chosen, it does follow precedent as a suggested way to differentiate dark-colored EuMN from light-colored PhMN.[8, 14] Conventional wisdom describes PhMN as a red-to yellow material synthesized in the presence of C. However, we have observed that the *in vitro* synthesis of MN in the presence of C leads to darker, more EuMN-like materials and that red-to-yellow materials can be obtained from L-DOPA and other precursors without the need for C.[15-16, 18] Given the exponential relationship between A and λ, an exponential relationship exists between k and A_{650}/A_{500} as shown in eq.2.

$$\frac{A_{650}}{A_{500}} = \frac{A_0 * e^{-k*650}}{A_0 * e^{-k*500}} = \frac{e^{-k*650}}{e^{-k*500}} = e^{-k*(650-500)} = e^{-k*150} \qquad \textbf{eq.2}$$

Figure 1 provides a graphical representation of **eq.2** and the "fluidity" of the visual appearances MN materials may exhibit independent of the presence of C. As discussed elsewhere[18] lower values of k tend to be associated with EuMN-like materials and higher values of k with PhMN-like materials in terms of their visual appearances.

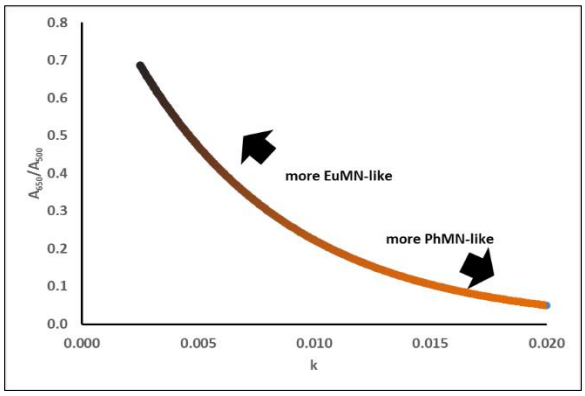

Figure 1: Relationship between decay constant k from **Eq.1** and the ratio of absorbance at 650nm over 500nm (A_{650}/A_{500}) to distinguish EuMN-like materials from PhMN-like materials according to **Eq. 2**.

For both reactions, absorbance spectra between 350 and 900nm were recorded of the crude mixtures at the end of the reaction and of their respective F_{disp} redispersed in water at 0.25

mg/mL. These spectra, normalized for their absorbance at 400nm, are shown in Figure 2, panel A. Figure 2, panel B, shows the absorbance spectra of both F_{disp} between 230 and 900nm, normalized for their absorbance at 250nm. Figure 2, panel C, shows the results of the evaluation of the EuMN-like or PhMN-like nature of the crude reaction mixtures and of the F_{disp} materials based upon their k and A_{650}/A_{500} values according to **Eq.**2 and as illustrated in Figure 1.

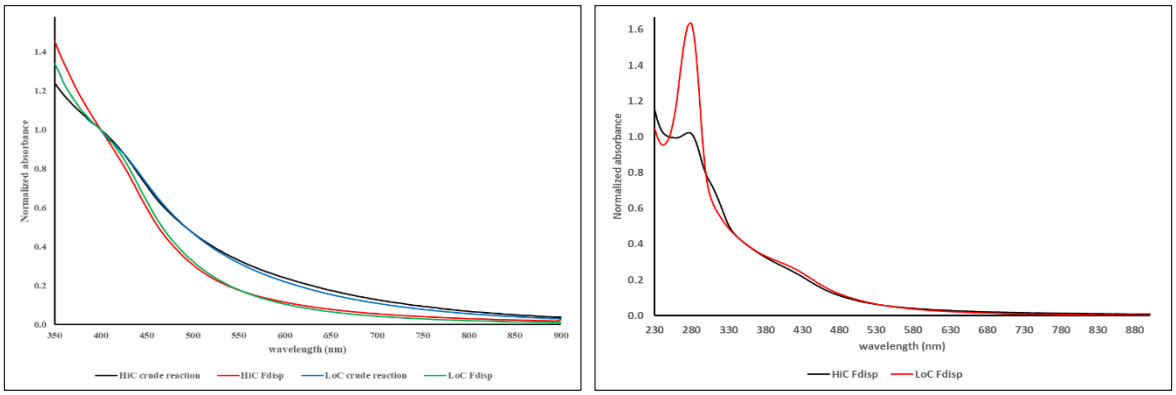

A **B**

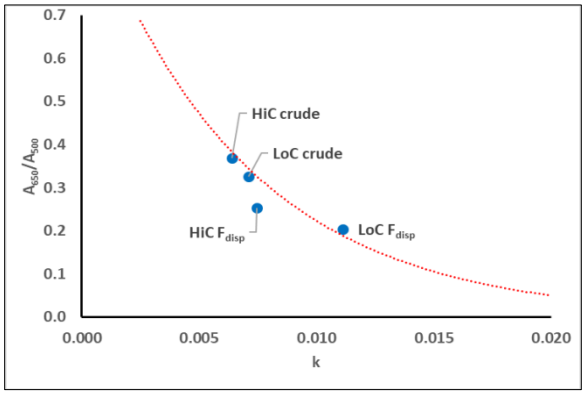

C

Figure 2: A: Vis spectra, normalized for their absorbance at 400nm, of the crude HiC and LoC reactions at the end of the reaction and of their respective F_{disp} redispersed in water at 0.25 mg/mL. **B**: UV-vis absorbance spectra, normalized for their absorbance at 250nm, of F_{disp} from both reactions redispersed in water at 0.25 mg/mL. **C**: Evaluation of the EuMN-like or PhMN-like characteristics of the crude reaction mixtures and of both F_{disp} based upon **Eq.2** and as outlined in Figure 1.

The absorbance spectra of both crude reaction mixtures were qualitatively similar, exhibiting exponential profiles, and this correlated with similar EuMN-like characteristics as judged from Figure 2, panel C. Little absorbance in the visible range was observed for both F_{disp} materials (see Figure 2, panel B). This correlates with a more PhMN-like appearance of these materials as judged from Figure 2, panel C. In the UV range, both F_{disp} fractions exhibited absorbance bands

centered around 280nm and 400nm (see Figure 2, panel B). However, clear quantitative differences appeared between both F_{disp} fractions. This observation may be responsible for the qualitative differences between both F_{disp} materials with F_{disp} from the LoC reaction exhibiting stronger PhMN-like characteristics (see Figure 2, panel C). The results associated with Figure 2 confirm earlier observations that the *in vitro* synthesis of MN leads to light-colored materials that are hidden behind the dark-colored, EuMN-like materials.[15-16]

3.1.2 HPLC profiles

Figure 3, panel A, shows the chromatographic profiles, viewed at 280nm, of the crude reaction mixtures and F_{disp} for both reactions. For qualitative comparisons the profiles are normalized for the absorbance of the main peak around 2.85min. Figure 3, panel B, shows the corresponding chromatographic profiles viewed at 400nm (raw data). Figure 3, panel C, shows the absorbance spectra of the two main peaks in these chromatographic profiles.

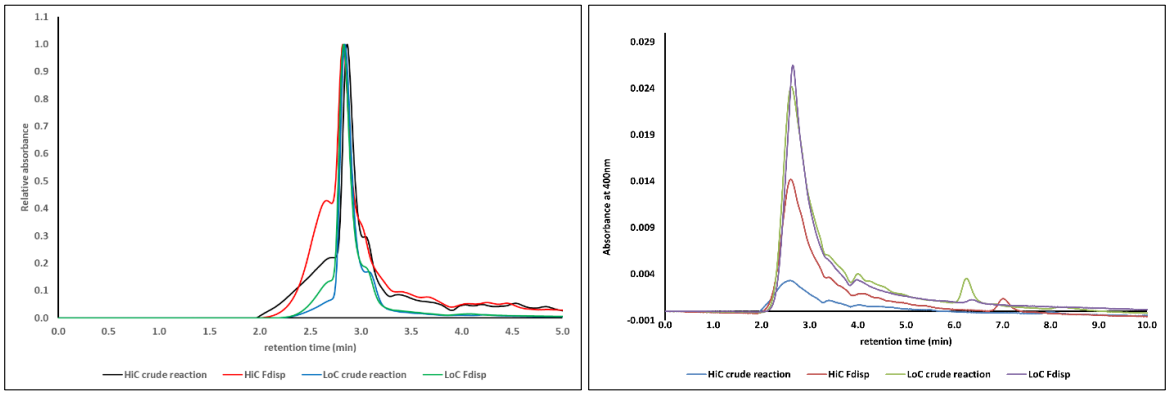

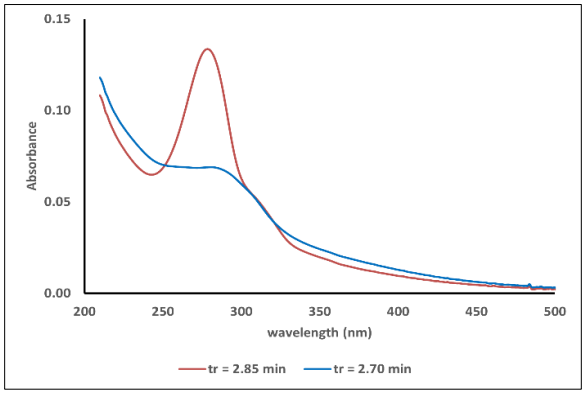

Figure 3: A: Normalized HPLC profiles at 280nm of the crude reaction mixtures and F_{disp} from both reactions**. B:** Raw data HPLC profiles at 400nm of crude reaction mixtures and F_{disp} from both reactions. **C:** Typical absorbance spectra of the two main peaks (retention times 2.7 and 2.85 minutes) in these HPLC profiles.

When viewed at 280nm (Figure 3, panel A) all HPLC profiles exhibit a combination of a broad peak (retention time between 2.65 and 2.70 min) and a dominant narrow peak (peak retention time around 2.85 min). Both peaks are poorly resolved and appear not to interact with the column as the solvent elution time was determined to be about 3.2 minutes. When viewed at 400nm (Figure 3, panel B) only a single, broad peak with a peak retention time between 2.65 and 2.70 minutes can be observed. For all materials, the absorbance spectra of the broad and narrow peaks are quantitatively different (Figure 3, panel C). These observations suggest that, for both reactions, the *in vitro* synthesis of MN from L-DOPA resulted in at least two sets of materials. One set contains the strong absorbance band at 280nm suggestive of unreacted precursor units. Another set contains the absorbance in the visible region and may be responsible for the visual appearance of the overall reaction mixture. These observations confirm earlier reports regarding the two-component aspect of *in vitro* synthesized MN.[15, 18-19]

The chromatograms shown in Figure 3 do suggest that quantitative differences in the relative abundance of both sets of materials exist between the HiC or LoC reactions. This indicates that reaction conditions could determine the ratio at which these two sets of materials are produced. The ratio of these two sets of materials may then impact the overall visual appearance and the physical stability of the reaction product. A hypothesis that has been suggested elsewhere.[15-16]

3.1.3 FT-IR spectra

Figure 4, panel A, shows the FT-IR spectra, normalized for their absorbance at 1,600 cm^{-1}, of the materials obtained from the HiC reaction. Figure 4, panel B, shows the corresponding spectra for the materials obtained from the LoC reaction. The spectra of the crude reaction mixtures were obtained after the dialysis and lyophilization of the crude mixtures but prior to their fractionation into F_{prec} and F_{disp}.

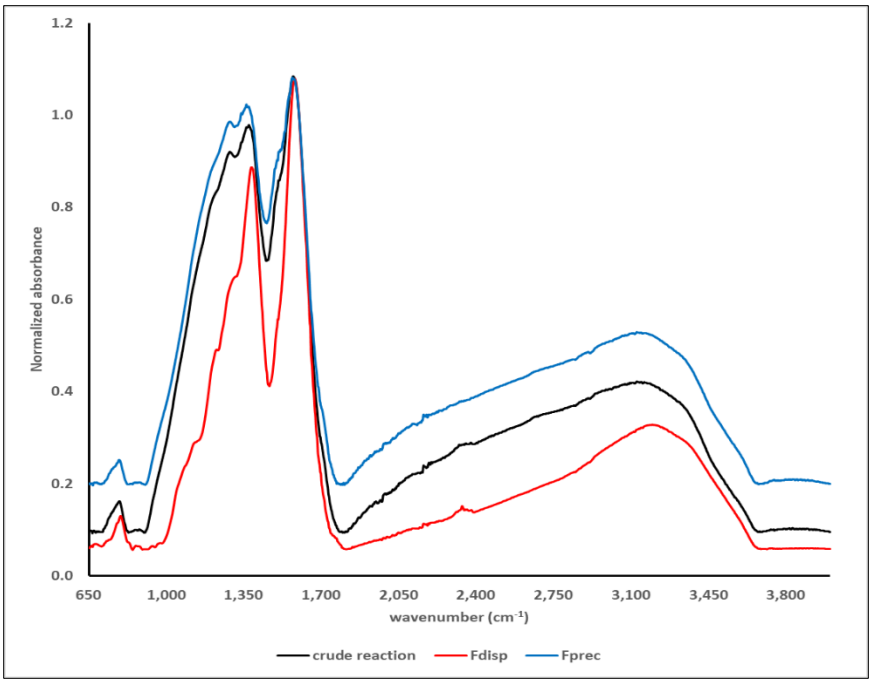

A

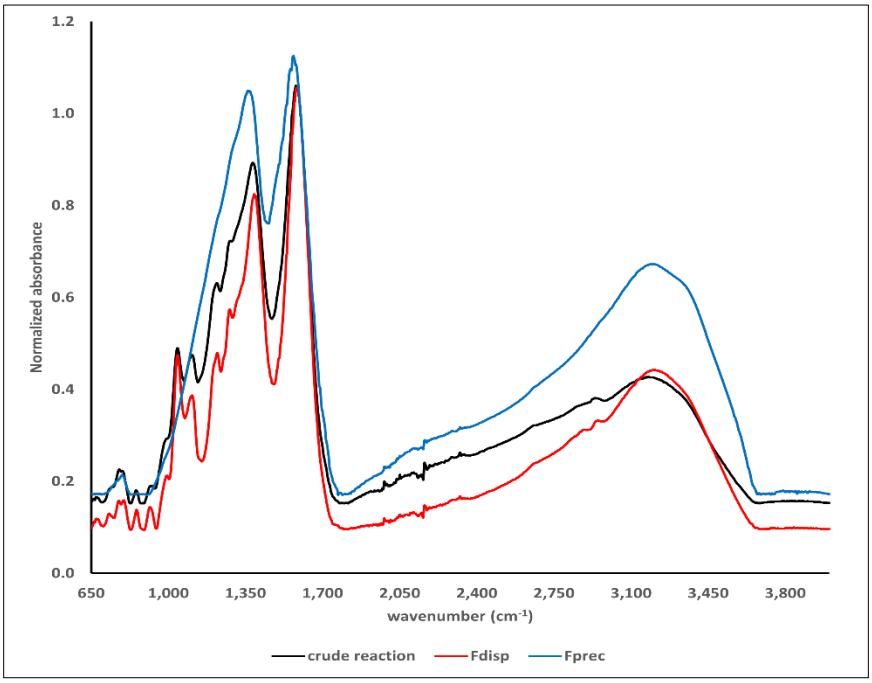

B

Figure 4: FT-IR spectra, normalized for their absorbance at 1,600 cm^{-1}, of materials obtained from HiC reaction (**A**) and LoC reaction (**B**).

Overall the FT-IR spectra exhibit the typical features of MN-like materials. Noticeably absent in these spectra is a signal around 1,700 cm^{-1} which would indicate the presence of a carbonyl group, e.g., from a carboxylic acid functional group. Such a signal was observed in L-DOPA-based materials that had undergone a wash with HCl.[16] This suggests that any carboxylic function may be present in carboxylate form, either through salt formation with Na^+ ions from the buffer or Na_2CO_3 or with *N*-containing entities within the synthesized structures. In addition, the lesser absorbance in the 1,000-1,400 cm^{-1} range of the fingerprint region of the F_{disp} material compared to the crude or F_{prec} materials is notable and has been observed before.[19]

3.2 Cation precipitation experiments with F_{disp} materials

Experiments involving F_{disp} from both reactions were set up as described in Section 2.3. Figure 5, panels A and B, shows the relationship between the cation concentration present in the precipitation mixture and the relative AUC of the supernatants for the F_{disp} material obtained from the HiC and LoC reaction respectively. The inserts in Figure 5 show the detailed results obtained for the cases of Cu^{2+} and Eu^{3+}. The results are presented as the relative AUC of the remaining supernatant compared to the sample with no added cation.

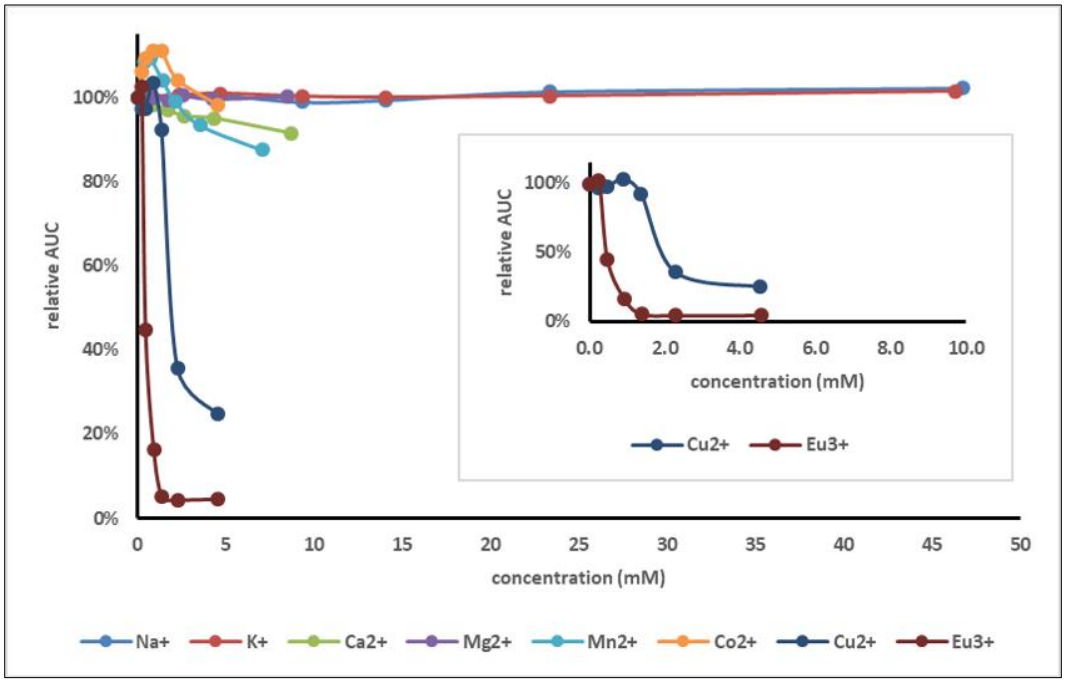

A

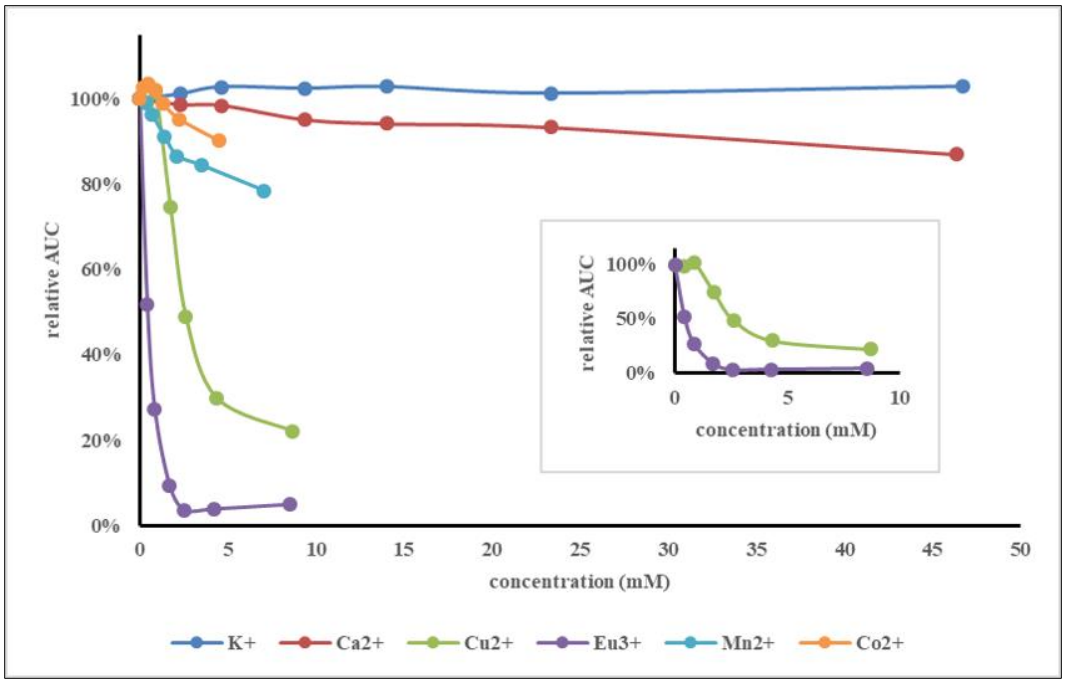

B

Figure 5: Relative AUC of the supernatants following precipitation of F_{disp} obtained from the HiC (**A**) or LoC (**B**) reaction with various cations. The insert details the results obtained for the cases of Cu^{2+} and Eu^{3+}.

Significant to total loss of color was achieved in the presence of sufficiently high concentrations of Cu^{2+} or Eu^{3+}. At higher concentrations, >100mM for Ca^{2+}, Mg^{2+} or Mn^{2+} and >200mM for Na^{+} or K^{+}, did the other cations induce significant precipitations of the colored materials. Nearly 100% loss of color in the supernatants was observed in the mixtures containing Cu^{2+} or Eu^{3+} tested at their highest concentrations. In the case of Cu^{2+} additional color due to the cation is present in the supernatants, but this did not alter the overall pattern of the results. The loss of color from F_{disp} did not decline linearly with increasing concentration of cation as illustrated in the inserts of Figure 5. This suggests that the F_{disp} materials are colloidal in nature as will be discussed later.

Figure 6 shows the HPLC profiles, normalized for the absorbance of the peak with retention time of 2.8min, obtained from the analyses of select supernatants following precipitations with Eu^{3+}.

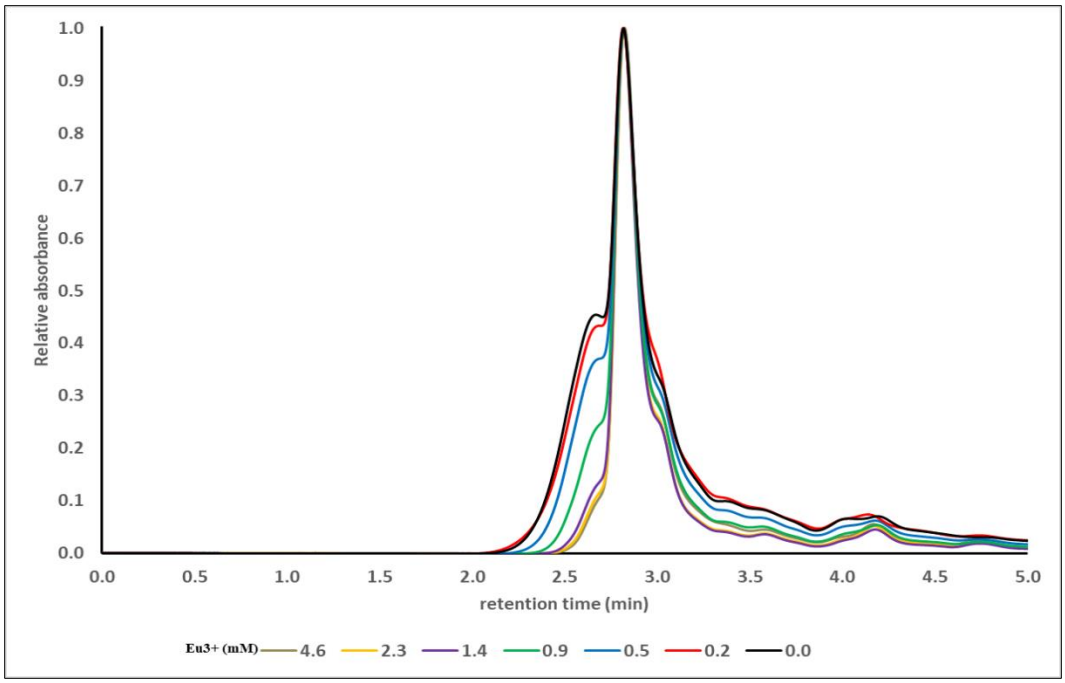

A

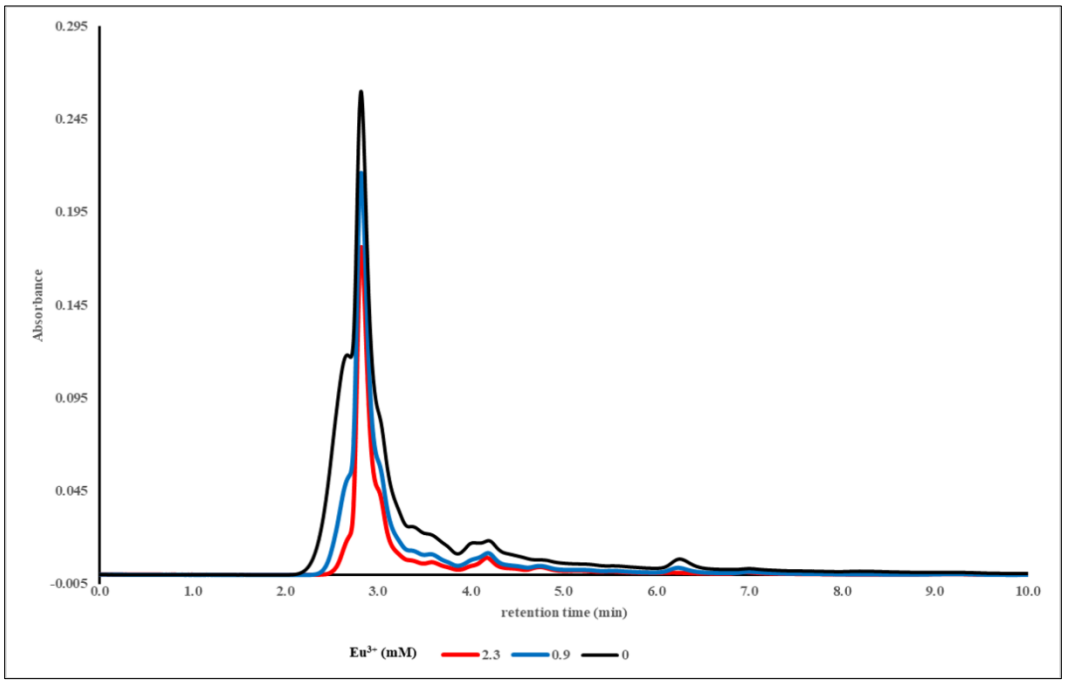

B

Figure 6: Normalized HPLC profiles of the supernatants following precipitation of F_{disp} obtained from the HiC reaction (**A**) or LoC reaction (**B**) with different levels of Eu^{3+}.

When precipitated in the presence of varying concentrations of Eu^{3+}, declines in the relevant peaks within the HPLC profiles were observed with increasing concentration of Eu^{3+}. Evaluating the HPLC profiles in a relative way it is observed that the broad peak with retention time around 2.6 minutes appeared to precipitate to a larger extent compared to the narrow peak with retention time around 2.85 minutes. This pattern of results was observed for F_{disp} from both reactions. In addition, it is noteworthy that, despite the total loss of color observed in some supernatants (see Figure 5), significant amounts of material appeared to remain in the supernatant samples as judged from the HPLC analyses. These observations confirm that the synthesis of MN results in a set of materials with strong absorbance in the UV range, but otherwise colorless (the F_{disp} fraction) in addition to the dark-colored substance generated (the F_{prec} fraction).

3.3 Dispersion of F_{prec} materials in KCl solutions

Figure 7, panels A through C, show results of the experiments set up as described in section 2.3 for F_{prec} obtained from the HiC reaction, while panels D through F show similar results for F_{prec} obtained from the LoC reaction.

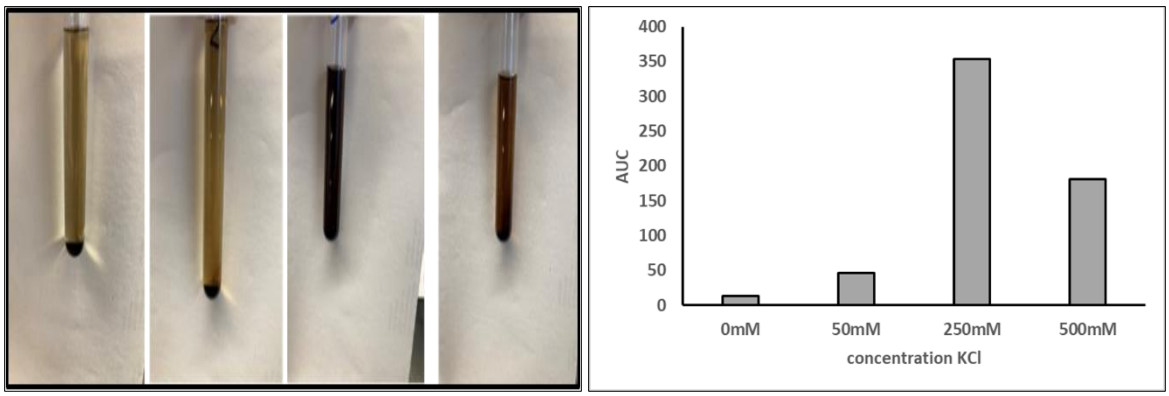

A **B**

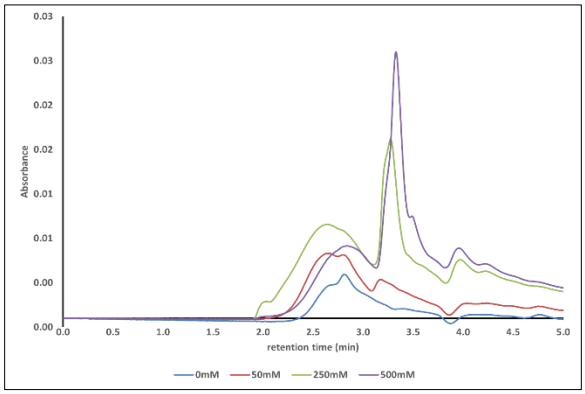

C

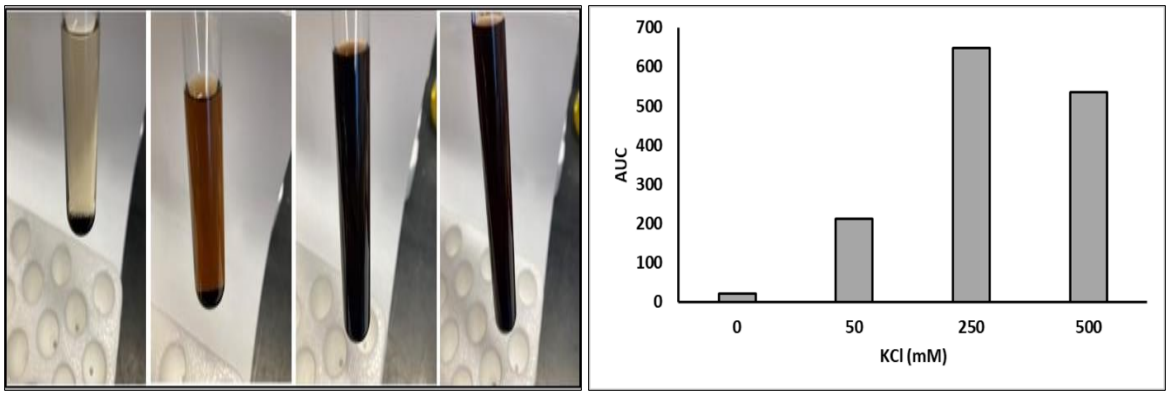

D **E**

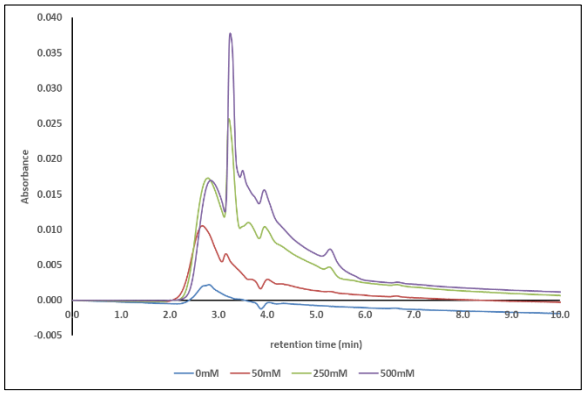

F

Figure 7: Dispersion of F_{prec} obtained from the HiC (**A** through **C**) or LoC (**D** through **F**) reaction in KCl solutions of different concentrations. **A** and **D**: photographs of the suspensions after overnight standing at room temperature (from left to right: 0mM, 50mM, 250mM and 500mM KCl). **B** and **E**: AUC values of supernatants shown in A or D. **C** and **F**: HPLC traces of supernatants shown in A or E.

The photographs shown in Figure 7, panels A and D, and the evaluation of the AUC values of the supernatants shown in Figure 7, panels B and E, illustrate that varying amounts of dark-colored materials were dispersed depending on the concentration of KCl involved. The chromatographic profiles shown in Figure 7, panels C and F, indicate that the material dispersed form F_{prec} consisted primarily of the compounds responsible for the broad band peak observed in the chromatographic profiles of the crude reaction mixture (see Figure 3) and little of the compounds responsible for the narrow peak with retention time of about 2.85 minutes. This observation is another indicator that the synthesis of MN resulted in a hybrid material with the F_{prec} material being distinctly different from the F_{disp} material. The chromatographic profiles

obtained of the supernatants involving 250mM and 500mM KCl show a distinct sharp peak with a retention time of about 3.3 minutes, but this peak was attributed to the presence of KCl.

4. Discussions

The results presented in this report confirm and expand our earlier observations regarding the hybrid nature of the products synthesized when generating MN-like materials *in vitro*.[15, 18] The current report provides some chromatographic evidence of the existence of the two sets of materials (see Figures 3 and 6). One set of materials is responsible for the overall dark appearance of the products and is not dispersible in deionized water. The other set exhibits little to no color, has a strong absorbance band around 280nm and readily disperses in deionized water. Apart from these physical differences, the FTIR spectra shown in Figure 4 indicate that chemical differences between F_{prec} and F_{disp} exist. Physical and chemical characterizations of some such materials have been performed recently.[19] The results of these studies were in line with the typical characteristics described for MNs. In the context of the current discussions, it is worthwhile to highlight the observations regarding the zeta potential measurements. These indicated that all materials are anionic species, with qualitative differences between the corresponding F_{disp} and F_{prec} materials.[19] In view of their anionic surface, it is not surprising that the MN materials behave as colloidal materials when mixed with different salts at different concentrations. The observed changes in physical stability (dispersion or precipitation) discussed here and elsewhere[15-16] can readily be explained by applying steric or electrostatic (de)stabilizing models as it relates to colloidal particles.[20] The similarities between our observations and the behavior of colloidal materials in general, make us conclude that the MN materials are colloidal particles in nature, even if the MN materials appear to be dissolved.

The notion that MN materials exist as colloidal particles is nothing new[21-25] but appears not systemically considered.[3, 26] Ionic strength is a parameter that is not carefully controlled during the synthesis or purification of MN materials unlike pH parameter. Measurements of the zeta-potential of the final product is not a general characterization parameter.[3] The notion that MN can be “dissolved” in NaOH or KOH solutions[10, 26-31] is to be questioned. Our experiments indicate that precipitated MN materials will disperse into homogenous mixtures upon the addition of KCl as long as sufficiently high concentrations of KCl are used. Throughout the literature there are anecdotal observations indicating the impact of changing ion concentrations

on the physical stability or instability of MN materials. Banerjee et al. have observed the "dissolution" of bacterial and other MN materials through the addition of Cu^{2+} or Zn^{2+}.[27] Multivalent cations like Cu^{2+} or the lanthanide cation series are known to bind to and precipitate MN.[25, 32] Balla et al. studied the oxidation of catechol by Cu^{2+} and observed the formation of a dark precipitate rich in Cu.[33] Binns et al. observed that DOPA-based MN could be precipitated by the addition of NaCl.[34] The size of the colloidal particles and the impact of the size on the properties of the colloidal particles is not the scope of this report. The main focus of this report is the observation that a colorless, stabilizing ligand is generated during the synthesis of MN colloidal particles. In the case of L-DOPA one can envision an ionic interaction between the stabilizing ligand and the aggregate because of the presence of *N*-containing and carboxylic acid functionalities. The observation that changes in ionic strength affect the interactions between stabilizing ligand and aggregate supports this vision. Thus, a hypothesis is proposed that the *in vitro* synthesis of MN-like materials leads to the generation of hybrid, colloidal particles. A dark-colored core (the F_{prec} fraction) stabilized by colorless ligands (the F_{disp} fraction). As suggested in an earlier report[15], reaction conditions may determine the ratio at which these two sets of materials are formed and that the ratio at which the F_{disp} and F_{prec} fractions are formed determines the physical appearance (light- or dark-colored) and the physical stability (dispersed or precipitated) of the overall MN material. The possibility that an aspect of the chemistry behind the synthesis of MN has been overlooked was recently raised.[35] In that research two chemically and physically distinct materials were generated from dopamine as the precursor.

Given the apparent physical, particulate nature of the MNs, it is worthwhile to reflect to what extent the physical properties of MN are due to their physical features (e.g., particle size, surface properties). A common characteristic of the MN class of materials is their capacity to absorb light over a broad range of the electromagnetic spectrum leading to monotonic absorbance profiles over the entire ultraviolet to near infrared region, a profile that can be fitted with an exponential equation.[36] Various explanations have been given to explain this shared property among MNs. In the chemical disorder model the observed absorbance profile is a result of the combined absorbances of a multitude of different individual molecular species.[37] A different model invokes the combination of different aggregated entities to explain the broad band absorbance; something that could be termed the physical disorder model.[38-41] Both models have been explored through experimental and computational approaches. An argument has been made

that the broad band absorption profile generated in the very initial stages of the reaction has charge-transfer (CT) characteristics due to an interaction between the precursor and its oxidized form.[39] Independent of whether chemical or physical aspects are responsible for the broad band absorbance, any model would have to explain why the result of the MN synthesis process is consistently "orderly"; consistently producing exponentially declining absorbance profiles. In recent years we have studied the synthesis of MN under varying reaction conditions including the addition of amino acids like C or others.[15-16, 18, 42] Throughout these studies we have never observed any deviations from the typical, exponentially declining absorbance spectra. In our observations, the only parameter that is influenced by the reaction conditions is the decay constant k present in **Eq.1**. It is the value of this constant that impacts the appearance of the material: dark or light colored; EuMN- or PhMN-like as shown in Figure 1. In general, it is worthwhile to compare the physic-chemical properties of MNs to the physic-chemical properties of graphene or graphene oxide and even to crude oil.[43-46] Similarly, it is worthwhile to compare the discussions on the nature of pigmentation in MNs to the discussions on the nature of pigmentation as it relates of food chemistry; particularly the topic of copigmentation.[47]

Conclusions

This report provides chromatographic and spectroscopic evidence that the *in vitro* synthesis of L-DOPA-based melanin leads to a hybrid material consisting of two sets of components. One set comprises the aggregated, dark material responsible for the overall visual appearance of the melanin material. The second set comprises a colorless, water-dispersible material that acts as a stabilizing ligand for the colloidal melanin particles. This colorless ligand displays strong absorbance in the UV range and can be dislodged from the aggregated core particles through the addition of cations with Cu^{2+} and Eu^{3+} being particularly effective.

Acknowledgements

VG and JW were supported by The Tennessee Louis Stokes Alliance for Minority Participation (TLSAMP) supported by the National Science Foundation (NSF – HRD 1826954).

References

1. Cao, W.; Zhou, X.; McCallum, N. C.; Hu, Z.; Ni, Q. Z.; Kapoor, U.; Heil, C. M.; Cay, K. S.; Zand, T.; Mantanona, A. J.; Jayaraman, A.; Dhinojwala, A.; Deheyn, D. D.; Shawkey, M. D.; Burkart, M. D.; Rinehart, J. D.; Gianneschi, N. C., Unraveling the Structure and Function of Melanin through Synthesis. *Journal of the American Chemical Society* **2021,** *143* (7), 2622-2637.

2. d'Ischia, M., Melanin-Based Functional Materials. *Int J Mol Sci* **2018,** *19* (1).

3. d'Ischia, M.; Wakamatsu, K.; Napolitano, A.; Briganti, S.; Garcia-Borron, J. C.; Kovacs, D.; Meredith, P.; Pezzella, A.; Picardo, M.; Sarna, T.; Simon, J. D.; Ito, S., Melanins and melanogenesis: methods, standards, protocols. *Pigm Cell Melanoma Res* **2013,** *26* (5), 616-33.

4. Maranduca, M. A.; Branisteanu, D.; Serban, D. N.; Branisteanu, D. C.; Stoleriu, G.; Manolache, N.; Serban, I. L., Synthesis and physiological implications of melanic pigments (Review). *Oncol Lett* **2019,** *17* (5), 4183-4187.

5. Mostert, A. B., Melanin, the What, the Why and the How: An Introductory Review for Materials Scientists Interested in Flexible and Versatile Polymers. *Polymers* **2021,** *13* (10).

6. Solano, F., Melanins: Skin Pigments and Much More:Types, Structural Models, Biological Functions, and Formation Routes. *New Journal of Science* **2014,** *2014*, 28.

7. Nasti, T. H.; Timares, L., MC1R, Eumelanin and Pheomelanin: Their Role in Determining the Susceptibility to Skin Cancer. *Photochemistry and Photobiology* **2015,** *91* (1), 188-200.

8. Ozeki, H.; Ito, S.; Wakamatsu, K.; Thody, A. J., Spectrophotometric Characterization of Eumelanin and Pheomelanin in Hair. *Pigment Cell Research* **1996,** *9* (5), 265-270.

9. Mason, H. S.; Wright, C. I., The chemistry of melanin; oxidation of dihydroxyphenylalanine by tyrosinase. *J Biol Chem* **1949,** *180* (1), 235-47.

10. Pal, A. K.; Gajjar, D. U.; Vasavada, A. R., DOPA and DHN pathway orchestrate melanin synthesis in Aspergillus species. *Medical Mycology* **2013,** *52* (1), 10-18.

11. Simon, J. D.; Peles, D. N., The Red and the Black. *Accounts of Chemical Research* **2010,** *43* (11), 1452-1460.

12. Fedorow, H.; Tribl, F.; Halliday, G.; Gerlach, M.; Riederer, P.; Double, K., Neuromelanin in human dopamine neurons: comparison with peripheral melanins and relevance to Parkinson's disease. *Prog Neurobiol* **2005,** *75* (2), 109 - 124.

13. Haining, R. L.; Achat-Mendes, C., Neuromelanin, one of the most overlooked molecules in modern medicine, is not a spectator. *Neural Regeneration Research* **2017,** *12* (3), 372-375.
14. Wakamatsu, K.; Nagao, A.; Watanabe, M.; Nakao, K.; Ito, S., Pheomelanogenesis is promoted at a weakly acidic pH. *Pigment Cell & Melanoma Research* **2017,** *30* (3), 372-377.
15. Vercruysse, K.; Govan, V., Melanogenesis: A Search for Pheomelanin and Also, What Is Lurking Behind Those Dark Colors?, *Preprint*, https://doi.org/10.26434/chemrxiv.11418075.v1, 2019
16. Vercruysse, K.; Govan, V., The yellow and the black of synthetic melanins, *Preprint*, https://doi.org/10.26434/chemrxiv-2021-h9dks, 2021
17. Vercruysse, K., Evaluating the "Darkness" of Melanin Materials, *Preprint*, https://doi.org/10.26434/chemrxiv.12762179.v1, 2020
18. Vercruysse, K.; Govan, V.; Harrison, J.; Caldwell, T.; Winford, J., Appearing as eumelanin or as pheomelanin and the push towards eumelanin by cysteine., *Preprint*, https://doi.org/10.26434/chemrxiv-2022-hcz2m, 2022
19. Galeb, H. A.; Eichhorn, J.; Harley, S.; Robson, A. J.; Martocq, L.; Nicholson, S. J.; Ashton, M. D.; Abdelmohsen, H. A. M.; Pelit, E.; Baldock, S. J.; Halcovitch, N. R.; Robinson, B. J.; Schacher, F. H.; Chechik, V.; Vercruysse, K.; Taylor, A. M.; Hardy, J. G., Phenolic Polymers as Model Melanins. *Macromolecular Chemistry and Physics n/a* (n/a), 2300025.
20. Stenkamp, V. S.; McGuiggan, P.; Berg, J. C., Restabilization of Electrosterically Stabilized Colloids in High Salt Media. *Langmuir* **2001,** *17* (3), 637-651.
21. Kohri, M.; Yanagimoto, K.; Kawamura, A.; Hamada, K.; Imai, Y.; Watanabe, T.; Ono, T.; Taniguchi, T.; Kishikawa, K., Polydopamine-Based 3D Colloidal Photonic Materials: Structural Color Balls and Fibers from Melanin-Like Particles with Polydopamine Shell Layers. *ACS Applied Materials & Interfaces* **2018,** *10* (9), 7640-7648.
22. Liu, Y.; Ai, K.; Liu, J.; Deng, M.; He, Y.; Lu, L., Dopamine-melanin colloidal nanospheres: an efficient near-infrared photothermal therapeutic agent for in vivo cancer therapy. *Adv Mater* **2013,** *25* (9), 1353-9.
23. Park, J.; Moon, H.; Hong, S., Recent advances in melanin-like nanomaterials in biomedical applications: a mini review. *Biomaterials Research* **2019,** *23* (1), 24.

24. Patil, A.; Heil, C. M.; Vanthournout, B.; Bleuel, M.; Singla, S.; Hu, Z.; Gianneschi, N. C.; Shawkey, M. D.; Sinha, S. K.; Jayaraman, A.; Dhinojwala, A., Structural Color Production in Melanin-Based Disordered Colloidal Nanoparticle Assemblies in Spherical Confinement. *Advanced Optical Materials* **2022,** *10* (5), 2102162.
25. Szpoganicz, B.; Gidanian, S.; Kong, P.; Farmer, P., Metal binding by melanins: studies of colloidal dihydroxyindole-melanin, and its complexation by Cu(II) and Zn(II) ions. *J Inorg Biochem* **2002,** *89* (1-2), 45-53.
26. Pralea, I.-E.; Moldovan, R.-C.; Petrache, A.-M.; Ilieș, M.; Hegheș, S.-C.; Ielciu, I.; Nicoară, R.; Moldovan, M.; Ene, M.; Radu, M.; Uifălean, A.; Iuga, C.-A., From Extraction to Advanced Analytical Methods: The Challenges of Melanin Analysis. *International Journal of Molecular Sciences* **2019,** *20* (16), 3943.
27. Banerjee, A.; Supakar, S.; Sheet, T.; Banerjee, R., Metal ion induced dissolution of melanin extracted from the bacterium *Azotobacter chroococcum*. *J. Indian Chem. Soc.* **2014,** *91*, 713-719.
28. Islam, A. T. M. R.; Shinzato, K.; Miyaoka, H.; Komaguchi, K.; Koike, K.; Arakawa, K.; Kitamura, K.; Tanaka, N., Isolation and characterization of blackish-brown BY2-melanin accumulated in cultured tobacco BY-2 cells. *Bioscience, Biotechnology, and Biochemistry* **2023,** *87* (4), 395-410.
29. Noman, A. E.; Al-Barha, N. S.; Chen, F., Characterization of Physicochemical Properties of Melanin Produced by Gluconobacter oxydans FBFS 97. *Fermentation* **2022,** *8* (11), 574.
30. Singh, S.; Nimse, S. B.; Mathew, D. E.; Dhimmar, A.; Sahastrabudhe, H.; Gajjar, A.; Ghadge, V. A.; Kumar, P.; Shinde, P. B., Microbial melanin: Recent advances in biosynthesis, extraction, characterization, and applications. *Biotechnol Adv* **2021,** *53*, 107773.
31. Suwannarach, N.; Kumla, J.; Watanabe, B.; Matsui, K.; Lumyong, S., Characterization of melanin and optimal conditions for pigment production by an endophytic fungus, Spissiomyces endophytica SDBR-CMU319. *PloS one* **2019,** *14* (9), e0222187.
32. Sarna, T.; Hyde, J. S.; Swartz, H. M., Ion-exchange in melanin: an electron spin resonance study with lanthanide probes. *Science* **1976,** *192* (4244), 1132-4.
33. Balla, J.; Kiss, T.; Jameson, R. F., Copper(II)-catalyzed oxidation of catechol by molecular oxygen in aqueous solution. *Inorganic Chemistry* **1992,** *31* (1), 58-62.

34. Binns, F.; King, J. A. G.; Mishra, S. N.; Percival, A.; Robson, N. C.; Swan, G. A.; Waggott, A., Studies related to the chemistry of melanins. Part XIII. Studies on the structure of dopamine-melanin. *Journal of the Chemical Society C: Organic* **1970,** (15), 2063-2070.
35. Mavridi-Printezi, A.; Giordani, S.; Menichetti, A.; Mordini, D.; Zattoni, A.; Roda, B.; Ferrazzano, L.; Reschiglian, P.; Marassi, V.; Montalti, M., The dual nature of biomimetic melanin. *Nanoscale* **2023,** *16* (1), 299-308.
36. Meredith, P.; Powell, B.; Riesz, J.; Nighswander-Rempel, S. P.; Pederson, M. R.; Moore, E. G., Towards structure-property-function relationships for eumelanin. *Soft matter* **2005,** *2 1*, 37-44.
37. Tran, M. L.; Powell, B. J.; Meredith, P., Chemical and Structural Disorder in Eumelanins: A Possible Explanation for Broadband Absorbance. *Biophysical Journal* **2006,** *90* (3), 743-752.
38. Chen, C.-T.; Chuang, C.; Cao, J.; Ball, V.; Ruch, D.; Buehler, M. J., Excitonic effects from geometric order and disorder explain broadband optical absorption in eumelanin. *Nature Communications* **2014,** *5* (1), 3859.
39. Mavridi-Printezi, A.; Menichetti, A.; Ferrazzano, L.; Montalti, M., Reversible Supramolecular Noncovalent Self-Assembly Determines the Optical Properties and the Formation of Melanin-like Nanoparticles. *The Journal of Physical Chemistry Letters* **2022,** *13* (42), 9829-9833.
40. Micillo, R.; Panzella, L.; Iacomino, M.; Prampolini, G.; Cacelli, I.; Ferretti, A.; Crescenzi, O.; Koike, K.; Napolitano, A.; d'Ischia, M., Eumelanin broadband absorption develops from aggregation-modulated chromophore interactions under structural and redox control. *Scientific Reports* **2017,** *7* (1), 41532.
41. Stark, K. B.; Gallas, J. M.; Zajac, G. W.; Golab, J. T.; Gidanian, S.; McIntire, T.; Farmer, P. J., Effect of Stacking and Redox State on Optical Absorption Spectra of Melanins−Comparison of Theoretical and Experimental Results. *The Journal of Physical Chemistry B* **2005,** *109* (5), 1970-1977.
42. Vercruysse, K.; Govan, V.; Fortner, S., Kinetic Study of the Melanogenesis from Select Catecholamines in the Presence of L-Cysteine or Other Amino Acids, *Preprint*, https://doi.org/10.26434/chemrxiv.12678860.v1, 2020

43. Di Capua, R.; Gargiulo, V.; Alfè, M.; De Luca, G. M.; Skála, T.; Mali, G.; Pezzella, A., Eumelanin Graphene-Like Integration: The Impact on Physical Properties and Electrical Conductivity. *Frontiers in Chemistry* **2019,** *7*.

44. Emiru, T. F.; Ayele, D. W., Controlled synthesis, characterization and reduction of graphene oxide: A convenient method for large scale production. *Egyptian Journal of Basic and Applied Sciences* **2017,** *4* (1), 74-79.

45. Ernestina Elizabeth Banda, C.; Nohra Violeta Gallardo, R.; Ulises Páramo, G.; Ana Maria Mendoza, M.; José Aarón Melo, B., Characterization of Crude Oils and the Precipitated Asphaltenes Fraction using UV Spectroscopy, Dynamic Light Scattering and Microscopy. In *Recent Insights in Petroleum Science and Engineering*, Mansoor, Z., Ed. IntechOpen: Rijeka, 2017; p Ch. 6.

46. Ojrzynska, M.; Wroblewska, A.; Judek, J.; Malolepszy, A.; Duzynska, A.; Zdrojek, M., Study of optical properties of graphene flakes and its derivatives in aqueous solutions. *Opt. Express* **2020,** *28* (5), 7274-7281.

47. Trouillas, P.; Sancho-Garcia, J. C.; De Freitas, V.; Gierschner, J.; Otyepka, M.; Dangles, O., Stabilizing and Modulating Color by Copigmentation: Insights from Theory and Experiment. *Chem Rev* **2016,** *116* (9), 4937-82.